Applied Energy 361 (2024) 122925

Contents lists available at ScienceDirect

Applied Energy

journal homepage: www.elsevier.com/locate/apenergy

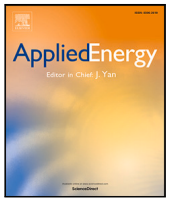

Assessing battery degradation as a key performance indicator for multi-objective optimization of multi-carrier energy systems

Lingkang Jin [a,*], Milad Kazemi [b], Gabriele Comodi [a], Christina Papadimitriou [b]

[a] Marche Polytechnic University, Department of Industrial Engineering and Mathematical Sciences, Ancona, Italy
[b] Electrical Engineering, Electrical Energy Systems, Eindhoven University of Technology, Eindhoven, Netherlands

ARTICLE INFO

Keywords:
Multi-objective optimization
Multi-carrier energy systems
Pareto curve
Battery degradation
State of health

ABSTRACT

The Pareto frontier is extensively adopted in multi-objective optimization, especially in multi-carrier energy system modeling. Despite the various methodologies available to derive the frontier, it represents different optimal solutions, making the final selection non-trivial. The modeler's expertise is crucial in determining the weight factors assigned to each objective for selecting the final solution from the Pareto frontier. This study proposes a novel approach to support such decision-making, introducing an additional key performance indicator, the state of health of the battery, evaluated through physical battery modeling. By comparing different scheduling schemes in multi-objective multi-carrier energy systems, each with its distinct battery operational strategy, this newly introduced indicator has deployed to automatically identify the ultimate solution from the Pareto frontier, without additional weighting coefficients. Such an approach, therefore, automates the decision process, which supports easy engineering, especially for the small scale multi-energy systems such as smart homes, like the case study presented in this work that has four distinct energy carriers, adopting the 12 V 128 Ah LFP chemistry Li-ion battery modules, demonstrates the effectiveness of this automated selection process. Furthermore, when compared to the maximum values across the entire frontier, the automatically chosen solution exhibits reductions of 27.96% in CO_2 emissions and 3.67% reduction in overall costs. Over long-term operation, this approach has the potential to extend battery lifespan by up to 26.67%, directly impacting the economics of multi-carrier energy systems.

1. Introduction

Energy systems modeling has a critical role as a support measure for energy planners and policymakers to deal with the complexities of the ongoing energy transition. As they undergo a profound transformation. Long-term energy planning is a key tool in anticipating and preparing for future energy scenarios, especially in light of the fluctuating and evolving energy policies [1]. Indeed, energy systems modeling provides a valuable framework for re-assessing and adapting to these dynamic conditions. Moreover, energy systems models are also instrumental in the operational stage, enabling the optimization of already installed energy assets based on the specific objectives set by the designer. This optimization can lead to improved scheduling and enhanced performance, ensuring the efficient utilization of available resources. By harnessing the power of energy systems modeling, decision-makers can make informed choices, and effective strategies, and drive the successful implementation of sustainable energy solutions.

Among the various approaches that enable energy transition, sector coupling emerges as a significant concept. It involves the integration of energy-consuming sectors with the power generation sector to effectively reduce energy transition costs [2]. The scientific literature presents many technical solutions for implementing sector coupling, with direct electrification of consumers and the utilization of Power-to-X technologies, as they enable cross-energy sector coupling, being particularly promising [3]. To effectively address the integration of sector-coupling measures, energy system modeling must be adjusted accordingly, to accommodate the infiltration of diverse energy networks. This means that multiple energy carriers and multiple objectives must be considered within energy systems modeling.

Certainly, the synergies among multiple energy carriers must be thoroughly evaluated, regardless of the scale of the multi-carrier system. With the proliferation of advanced and energy-efficient buildings, which incorporate various energy carriers, these modern constructions, often referred to as "smart homes", can also be effectively modeled as multi-energy systems. These smart homes are equipped with a range of intelligent technologies designed for producing, converting, storing, and consuming energy. These technologies are seamlessly managed

* Corresponding author.
E-mail address: l.jin@pm.univpm.it (L. Jin).

https://doi.org/10.1016/j.apenergy.2024.122925
Received 17 October 2023; Received in revised form 1 February 2024; Accepted 23 February 2024
Available online 27 February 2024

Nomenclature

Acronyms

ACh	Absopriont Chillers
BCD	Basic Cooling Demand
BESS	Battery Energy Storage Systems
BHD	Basic Heating Demand
BNGD	Basic Natural Gas Demand
CC-CV	Constant Current-Constant Voltage
DFN	Doyle-Fuller-Newman
ECM	Equivalent Circuit Model
EV	Electric Vehicles
FEL	Flexible Electrical Loads
HEMS	Home Energy Management System
HP	Heat Pump
LFP	Lithium iron phosphate
MAE	Mean Absolute Error
MILP	Mixed Integer Linear Programming
NCA	Nickel Cobalt Aluminum
NMC	Nickle Manganese Cobalt oxide
PBM	Physic-Based Model
PS2D	PSeudo Two Dimensional model
PV	PhotoVoltaic systems
PyBaMM	Python Battery Mathematical Modeling
RHS	Right Hand Side
SCD	Space Cooling Demand
SHD	Space Heating Demand
SOH	State Of Health
SPM	Single Particle Model
SPMe	Single Particle Model with Electrolyte
ST	Solar Thermal systems
TSEL	Time-Shiftable Electric Loads
TSS	Thermal Storage Systems

Sets

t	Timesteps

Parameters

Δt	Timestep length per hour
$\eta^{BESS,ch}$	Discharging efficiency of BESS
$\eta^{BESS,dis}$	Charging efficiency of BESS
$\lambda_t^{g,b}$	Natural gas energy buying price, [€/Nm^3]
$\lambda_t^{h,s}$	Heating energy selling price, [€/kWh]
$\lambda_t^{h,b}$	Heating energy buying price, [€/kWh]
$\lambda_t^{p,b}$	Electric energy buying price, [€/kWh]
$\lambda_t^{p,s}$	Electric energy selling, [€/kWh]
ξ	Carbon intensity of energy consumption, [kg$_{CO_2}$/kWh]
LHV_g	Lower heating value of gas, [kWh/Nm^3]
N	Number of cells
n	Number of Pareto curve solutions
$r^{BESS,ch}$	Charging rate of BESS, [kW]
$r^{BESS,dis}$	Discharging rate of BESS, [kW]
$soe^{BESS,ini}$	Initial state of charge for BESS, [kWh]
$soe^{ESS,min}$	Minimum state of charge for BESS, [kWh]
$soe^{ESS,max}$	Maximum state of charge for BESS, [kWh]

Subscripts

$batt$	Battery module level
$cells$	Cell level
$parallel$	Parallel connections
$series$	Series connections

Variables

$p_t^{BESS,dis}$	Power discharged from BESS, [kW]
$p_t^{BESS,s}$	Power sold to external grid from BESS, [kW]
u_t^{ESS}	Binary variable for BESS
E	Energy, [kWh]
$g_t^{ext,b}$	Natural gas bought (import) from the network, [m^3]
$h_t^{ext,b}$	Heating power bought (imported) from the external grid, [kW]
$h_t^{ext,s}$	Heating power sold (exported) to the external grid, [kW]
$p_t^{BESS,ch}$	Power charged for BESS, [kW]
$p_t^{BESS,u}$	Power used internally from BESS, [kW]
$p_t^{ext,b}$	Electric power bought (imported) from the external grid, [kW]
$p_t^{ext,s}$	Electric power sold (exported) to the external grid, [kW]
Q	Capacity, [Ah]
soe_t^{BESS}	State of charge for BESS, [kWh]
T	Temperature, [K]
V	Voltage, [V]

by a Home Energy Management System (HEMS), which operates in response to dynamic pricing structures and carbon dioxide (CO_2) signals transmitted by the power grid, as outlined in the study by Fiorini et al. [4].

While financial and environmental objectives are commonly pursued in energy systems optimization, several other objectives can also be selected. For instance, minimizing grid dependency, reducing dumped energy, or maximizing energy reliability are additional objectives, that have been identified in the work of Khezri et al. [5]. The vast amount of objectives reflects the requirement to extend the scope of energy system optimization to multi-objective driven. By adopting sector coupling and following a comprehensive approach to energy system modeling, policymakers, and energy planners can deal with the complexities of the energy transition more effectively. Indeed they can identify optimal solutions that balance financial viability, environmental sustainability, grid resilience, and other relevant objectives. When there are multi-objectives to optimize, a trade-off among them has to be found, and there are different techniques to find the set of the trade-off solutions, among different techniques, ϵ-constraint method proposed by Mavrotas [6], and weighted sum method, are the most adopted ones by scientific community [7]. And as a result of both methods, the Pareto curve or Pareto frontier is obtained.

The Pareto curve is a graphical representation of non-dominated solutions in a multi-objective optimization problem. Each point on the curve represents a solution that is optimal in the sense that no other solution is better for all objectives. However, selecting the "ultimate" solution from the Pareto front depends on the decision maker's preferences and priorities among the different objectives. One way to select the best solution from the Pareto front is to use a decision-making method that incorporates the decision maker's preferences, such as weighting coefficients for objective functions or a utility function approach [5]. Another way is to use an interactive method where the decision maker provides feedback on the solutions presented and the algorithm generates new solutions based on this feedback. It is crucial to

recognize that determining the "best" solution is subjective and reliant on the decision maker's priorities and preferences. This subjectivity introduces the possibility of implicit biases, emphasizing the importance of aligning the decision-making process with the decision-maker's expertise and experience.

Wang et al. [8] have analyzed such aspects, indeed, they have compared 10 different methods, adopted for chemical engineering, each of them to select the best solution on the Pareto curve. among them, only the Gray Relational Analysis method does not require the weight functions, i.e. does not require additional inputs from designers to select the best solution. As specifically dedicated to energy systems modeling, Khezri et al. [5] have investigated both stand-alone and grid-connected energy systems. Among different perspectives, they have discussed the customer satisfaction index, in front of demand-side management measures, or grid dependency indicator, as a performance indicator for selecting the best solution of the Pareto curve; Concluding that battery characteristics are still left out from multi-objective optimization, due to its complexity and the lack of the suitable tools, indicating that there is still a research gap in such sense.

Over the years, many researchers have investigated Li-ion battery numerical modeling, primarily for automotive applications [9], to boost electrical vehicle penetration. There are two main branches of battery models, Equivalent Circuit Models (ECM) and Physical-Based Models (PBM) according to the review paper of Zhao et al. [10]; Where ECMs deal with the battery based on an equivalent electrical circuit, using basic electrical components like resistors and capacitors to model the battery behavior. As a consequence, they are easy to implement and fast to solve, however, they lack accuracy for real-life battery applications, especially in dynamic operations. PBMs instead, can deliver a higher accuracy since they treat the battery physic phenomena, including Butler–Volmer kinetic equations [11,12], they gave insights about the internal dynamics of batteries such as Li-ion diffusion, Ohmic effects, and electrochemical kinetics, and therefore they make possible to assess battery degradation possible. To make the PBMs even more accurate, more and more researchers are adopting data-driven and machine-learning techniques [13], however, they would require a large amount of test data, which quite often is not possible to have.

The aim of this work is, to propose a novel approach, which assesses the State of Health (SOH) of the battery, through a Li-ion battery physical modeling framework (*Pybamm* [14]), characterized by the battery manufacturer datasheet data, i.e. no experimental testing on the battery is required, due to different multi-objective scheduling operational strategies, each of them is a solution from Pareto curve, assessed from HEMS, of a smart home case, where four distinct energy carriers and its related systems are included, and finally obtain automatically the best solution, without any additional input from modelers.

The main contributions of this paper are summarized as follows:

1. The physical model of the battery is characterized using the data provided by the battery datasheet, declared by the manufacturer, sometimes even accessible online, meaning that the battery testing is not mandatory and the assessment can be done before the battery investment.
2. Both electrical and thermal properties, of the Li-ion battery are included, thus also their coupled phenomena are captured, in order to calculate the SOH indicator.
3. The Li-ion battery is fully parameterized, using experimental data declared by the battery manufacturer, supported by numerical assessment, which allows evaluation of many operational parameters of the battery, often neglected in ECMs, such as charging mode, voltage fluctuation, C-rate, temperature, etc.
4. Automatic selection of the best solution for the Pareto curve, without any further indications from the modeler who has built up the optimization, i.e. no weighting functions of objectives are needed to select the best solution.

The rest of the paper is organized as follows: In Section 2, the *Pybamm* framework and the parameterization process of the Li-ion battery are firstly discussed, to be followed by a description of HEMS, illustrating how multiple objectives are reported; And finally, the process to adopt SOH as an indicator is reported. Results and comments are in Section 3 to be concluded with Section 4 .

2. Material & methods

In this section, firstly the Pybamm framework and the battery parameterization concept is discussed, followed by the whole work methodology. Which is divided into three subsequent phases, that are (i) battery parameterization, (ii) Pareto curve solutions from HEMS, and finally (iii) the automatic selection of the best solution from them using the SOH as an indicator. Each phase is described in detail in the following subsections.

2.1. Pybamm framework

PyBaMM (Python Battery Mathematical Modeling) is an open-source battery simulation package written in Python, and developed by a team of experts, funded by the British funding scheme, the Faraday Institution [15] and NumFOCUS [16]. The whole repository of the project can be found on the GitHub page at [17]. It provides a framework for writing and solving systems of differential equations, a library of battery models and parameters, and specialized tools for simulating battery-specific experiments and visualizing the results. Furthermore, different physics-based electrochemical models are included, like Doyle–Fuller–Newman (DFN) and also the Single Particle Model with Electrolyte (SPMe), proposed by Marquis et al. [18], using state-of-the-art automatic differentiation and numerical solvers, such as CasADi [19], indeed multiple scientific papers are produced by the same developers, describing the framework modeling process, covering all aspects considered [18,20–24]. All models are implemented flexibly, and a wide range of models and parameter sets are available. Is also possible to set specified drive cycles of the battery, using user-defined current, voltage, or power curves.

There are other battery simulation projects similar to PyBaMM, such as PETLION and COMSOL Multiphysics [25]. While PETLION is an open-source software, written in Julia coding language, for millisecond-scale porous electrode theory-based lithium-ion battery simulations [26]. COMSOL Multiphysics, instead, is a commercial software for solving PDEs using the finite element method and offers an additional battery simulation module, including lithium-ion, lead–acid, nickel-metal hydride (NiMH), vanadium redox flow, and soluble lead–acid flow batteries.

PyBaMM stands out due to its flexibility, modularity, and open-source nature. Its use of Python as the coding language has attracted a more extensive research community, resulting in more comprehensive documentation compared to its Julia-based counterpart. Moreover, it is a modular framework that allows for quick model interchangeability, making it valuable in different stages of battery research and development. The framework is open source, which means anyone can use, modify, and distribute it, enhancing global battery technology research. PyBaMM's comprehensive model library includes a wide range of physics-based models, making it a vital tool in diverse battery research.

2.2. Battery parameterization

The parameterization of the Li-ion battery is the process of including the Li-ion battery characteristics into the Pybamm framework so that it can reproduce the battery's operational properties accurately, even under different operating conditions. Parameterization, therefore, has a fundamental role in the proper assessment of battery degradation under different operating conditions, and it is divided into two steps,

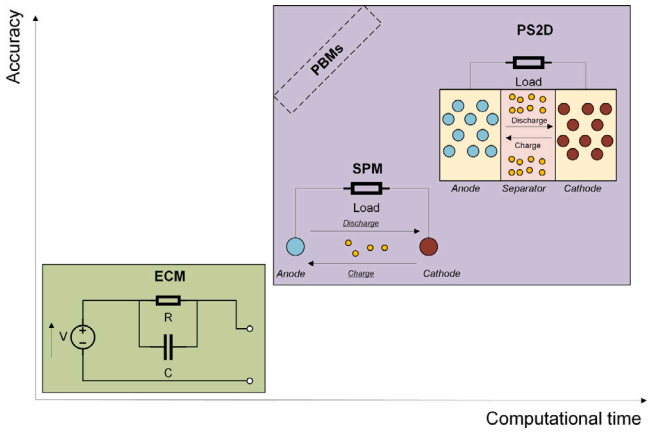

Fig. 1. Battery numerical models comparison. ECMs offer quick solutions but compromise on accuracy. Conversely, PBMs deliver higher accuracy, albeit at the expense of increased computational effort.

initialization and parameters tuning, which is based on the experimental data, that the battery manufacturer can provide, stated in datasheets. The PyBaMM framework provides various parameter sets that are validated by developers and contributors [27]. It is crucial to recognize that these sets might not be universally applicable to every battery on the market. Therefore, this work addresses the necessity of parametrizing new battery sets using data extracted from manufacturers' datasheets, as elaborated in the following sections. The reason for the mandatory parameter tuning in this work is twofold. Firstly, while other researchers have undertaken similar endeavors, such as extracting parameters from batteries and updating them into the PyBaMM database, these efforts often demand a deep understanding of electrochemistry expertise not commonly possessed by energy system modelers. Extracting a vast amount of electrochemical and material details [27] is complex and often not openly accessible, rendering the process challenging. To overcome these challenges of complexity and data availability, the parameterization approach presented in this work adopts a data-driven tuning approach, often used by modelers. This involves using similar sets of batteries as a starting point (initialization) and employing commonly used techniques such as the minimization of Mean Average Error.

2.2.1. Cell level model initialization

The first step of the parameterization is the initialization of the Pybamm model using the datasheet's operational data, reported by Li-ion battery manufacturers:

1. Battery chemistry, which can be Lithium iron phosphate (LFP), Nickel Manganese Cobalt oxide (NMC) or Nickel–cobalt–aluminum (NCA). And based on the chemistry, the Modelers can select among the built-in parameter sets from the Pybamm framework, all of them can be consulted at [27].
2. Charging mode, although almost every manufacturer is adopting Constant Current-Constant Voltage (CC-CV) mode, is possible to have some exceptions.
3. Electrode geometry, which is crucial to assess the electrical properties such as current densities, however, this information is not often reported in the datasheet.

From the modeler's perspective, the numerical model for the battery has to be selected, among different available ones, with the increasing physics details, but also the computational burden, as illustrated in Fig. 1. The ones based on physics are Single Particle Model (SPM) [18], Single Particle Model with electrolyte (SPMe) [18], Doyle–Fuller–Newman Model or Pseudo Two Dimensional (PS2D) [11].

The entire initialization process is reported in Fig. 2, and once completed, is already possible to perform experiments and assess the operational behavior of the Li-ion battery, however, since the parameter set is based on the built-in ones, some of the properties may differ from the ones from the datasheet, the reason why the second step of the parameterization is needed.

2.2.2. Parameters tuning

As the second step of the parameterization, different parameters of the model have to be tuned, in order to fit the experimental data, provided by battery manufacturers. The whole workflow is represented graphically in Fig. 7. From the datasheet provided by battery manufacturers, the following lab test results are normally reported:

1. Discharge curves at different C-rates.
2. Discharge curves at different temperatures.
3. Aging/degradation curves at 1-C cycles.

The parameters tuning is not trivial, since it is not straightforward which parameters to tune in order to have the best accuracy, compared with the experimental data. Additionally, thermal and electrical properties are strictly connected, by the kinetics of the electrode, governed by the Butler-Volmer equation, hence, making the parameters tuning even more arduous and complex. However, it is not impossible, and in this work, a data-driven approach, through the use of Mean Absolute Error (MAE) as an index, widely adopted in the machine learning research field, has been adopted. The process is illustrated in Fig. 3, and it has two steps:

1. Sensitivity analysis, of all tunable parameters, changing them from the default value and twice its original value, and observing the variation of MAE; Generally speaking, for proper sensitivity analysis, more data points of the parameters should be assessed, yet, with the vast amount of parameters to be evaluated, the computational effort would be enormous.
2. Selection of the most important parameters based on the previous step, and through the grid-search method, where all selected parameters are defined within their own range, based on the physical meaning of the parameter, to finally obtain the values of the selected parameters, that minimize the MAE.

Despite the intrinsic link between electrochemical and thermal properties, included in the Pybamm, for the sake of this work's scope, their parameterization can be decoupled, making the whole process easier. Indeed, the electrochemical experiments are done at a constant, standard temperature of 25 °C/298 K, where the thermal properties are not subject to any variation. Subsequently, aging parameterization can proceed as it requires the outputs of the electrochemical one. Furthermore, the aging part requires an extended experiment, i.e. more than 2000 cycles of charging and discharging, meaning that it requires more computational time, compared to the other two parameterization steps. Thus, the whole parameters tuning is sequential consisting of the following steps: (1) electrochemical parameterization, (2) thermal parameterization, and finally (3) aging parameterization, as illustrated in Fig. 4.

2.3. HEMS

The HEMS obtains the optimal real-time scheduling of domestic appliances by acquiring the forecasting of the loads, ambient temperature, solar irradiance, and information about the mobility of electric vehicles (EVs), based on historical data, as reported in Fig. 5. As can be seen, the peak demands are 0.50 kW for electricity, 0.185 Nm^3 for gas, 2.5 kW for heat, and 0 Nm^3 for hydrogen. Which indicates that no hydrogen-based appliance is present.

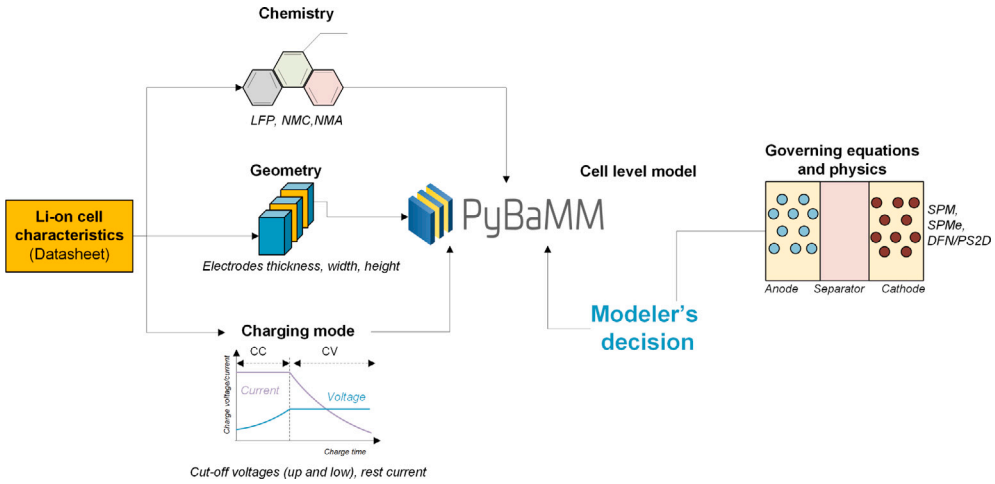

Fig. 2. Workflow of the initialization of Pybamm model. Cell details such as chemistry (LFP, NMC, etc.), geometry, and charging mode data are extracted from the datasheet. Modelers have the flexibility to choose the appropriate physics-based model for their application.

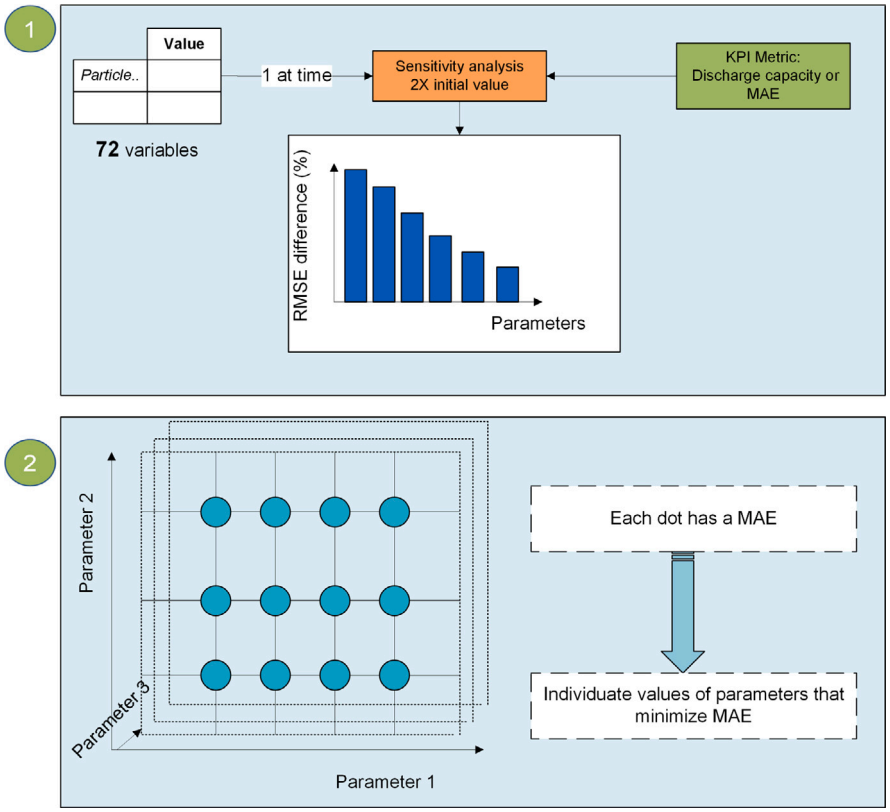

Fig. 3. Parameters selection and tuning process. The process of parameter selection and tuning involves an initial analysis of the impact of all tunable variables (72) on discharge capacity. The focus is on identifying the variables with significant importance, which are then subjected to the tuning process.

The real-time scheduling, with 15 min resolution, requires the HEMS to be modeled in a simple, yet efficient way. Therefore, a mixed-integer linear programming-based (MILP) model is developed to embrace the functionality of the appliances [28]. The design architecture of the proposed multi-carrier HEMS is illustrated in Fig. 6.

Accordingly, the proposed HEMS is composed of two renewable energy sources, with solar irradiance being the primary source, yet delivering different energy carriers, Photovoltaic (PV) and Solar Thermal (ST) systems. Two static energy storage systems, Battery Energy Storage Systems (BESS) and Thermal Storage Systems (TSS) are designated for electricity and heating carriers respectively, and EV is also present in the system with similar behavior to the BESS, using the Vehicle-to-Grid approach, during its availability. The interconnection between multiple carriers is made possible through energy conversion technologies. Accordingly, the Heat Pumps (HP) and Absorption Chillers (ACh) interconnect heating and internal cooling energy carriers to establish the interplay between the electricity and heating sectors. Also, as the architecture suggests the bidirectional energy exchange between the HEMS and external energy carrier is only available for electricity and district heating carriers. Furthermore, controllable appliances such as Time-Shiftable Electric Loads (TSEL), Space Cooling Demand (SCD) and Space Heating Demand (SHD), can provide the HEMS with further flexibility throughout the day.

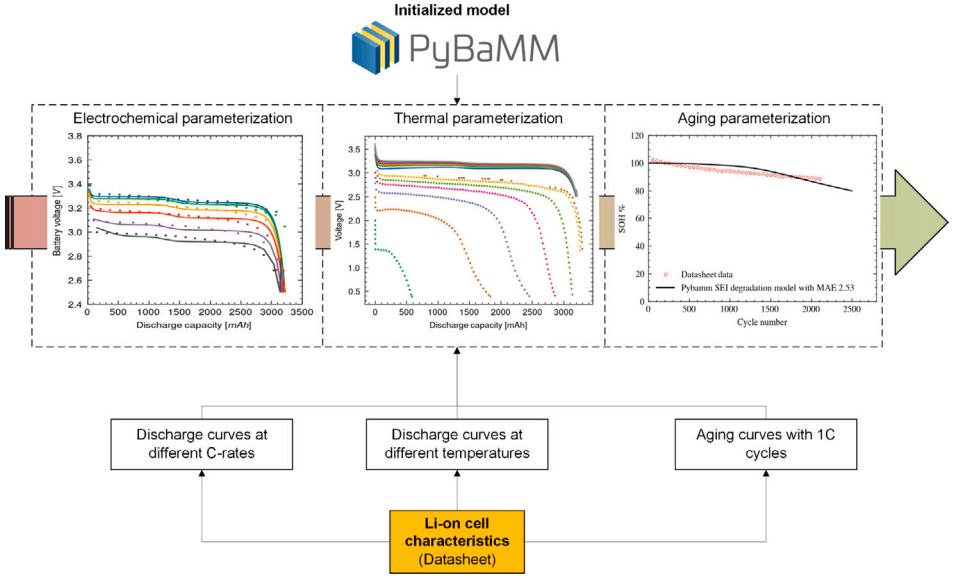

Fig. 4. Workflow of the parameters tuning for Pybamm model: (1) electrochemical parameterization, assessed using experimental discharge curves at different C-rates at 298 K, (2) thermal parameterization, where discharge curves at different temperatures at 1C are adopted, and finally (3) aging parameterization, using complete cycles at 1C, with 298 K temperature. As a result of this, the Pybamm model is ready to predict the battery behavior under other working conditions.

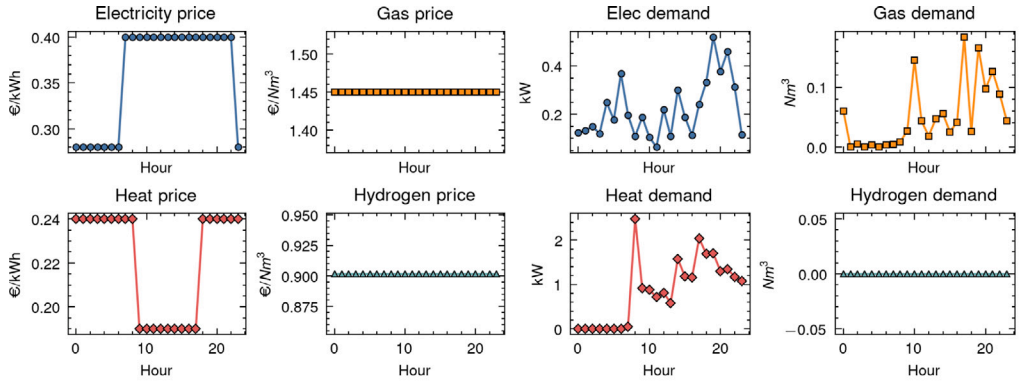

(a) Energy prices variation during the operational day. (b) Energy demands variation during the operational day.

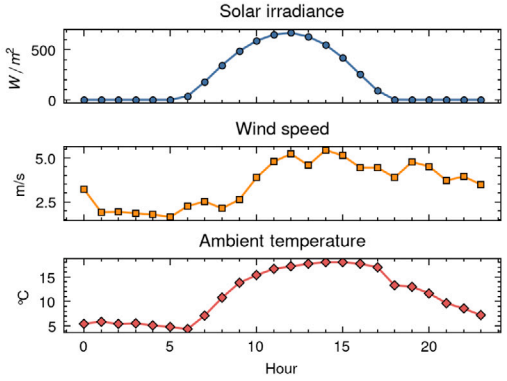

(c) Enviromental conditions variation during the operational day.

Fig. 5. Home monitored historical data. Based on these data it is possible to forecast and schedule.

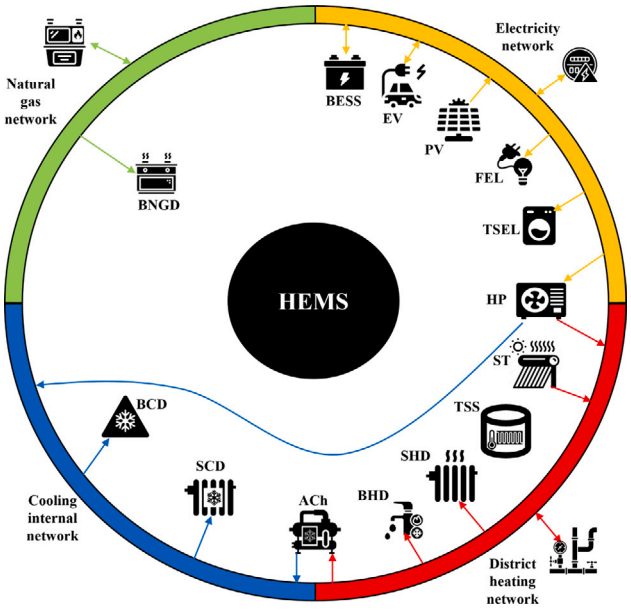

Fig. 6. Design architecture of proposed multi-carrier HEMS [28].

The HEMS as the mastermind schedules the controllable appliances present in the system to accomplish two objectives, minimizing the operational cost, and mitigating the negative environmental impacts by reducing the CO_2 emission. Therefore, the model incorporates a bi-objective MILP model. The methodology proposed in this literature is a follow-up to work presented in [28] where the complete mathematical modeling for the appliances could be found. However, since the focus of this work is mainly on the health improvement of BESS by accounting for a multi-objective function, the objective functions and BESS model are provided in the following.

$$\min Cost = \sum_{t\in\mathcal{T}} \left\{ \lambda_t^{p,b} p_t^{ext,b} - \lambda_t^{p,s} p_t^{ext,s} + \lambda_t^{h,b} h_t^{ext,b} - \lambda_t^{h,s} h_t^{ext,s} + \lambda_t^{g,b} g_t^{ext,b} \right\} \Delta t \tag{1a}$$

$$\min \mathrm{CO}_2 = \sum_{t\in\mathcal{T}} \xi \left\{ p_t^{ext,b} + h_t^{ext,b} + g_t^{ext,b} LHV_g \right\} \Delta t \tag{1b}$$

$$s.t. \quad p_t^{BESS,u} + p_t^{BESS,s} = \eta^{BESS,dis} p_t^{BESS,dis} \quad \forall t \in \mathcal{T} \tag{1c}$$

$$0 \le p_t^{BESS,ch} \le r^{BESS,ch} u_t^{BESS} \quad \forall t \in \mathcal{T} \tag{1d}$$

$$0 \le p_t^{BESS,dis} \le r^{BESS,dis} (1 - u_t^{BESS}) \quad \forall t \in \mathcal{T} \tag{1e}$$

$$soe_t^{BESS} = soe_{t-1}^{BESS} + \eta^{BESS,ch} p_{t-1}^{BESS,ch} \Delta t - p_{t-1}^{BESS,dis} \Delta t \quad \forall t \in \mathcal{T} - \{t_0\} \tag{1f}$$

$$soe_t^{BESS} = soe^{BESS,ini} \quad \forall t = t_0, t_n \tag{1g}$$

$$soe^{BESS,min} \le soe_t^{BESS} \le soe^{BESS,max} \quad \forall t \in \mathcal{T} \tag{1h}$$

$$Remainder\ of\ model\ equations\ coming\ from [28] \tag{1i}$$

Accordingly, Eqs. (1c)–(1h) represents the BESS model. In the model, the simultaneous charging and discharging of the battery is prohibited by Eqs. (1d) and (1e) using an auxiliary binary variable, u_t^{ESS}.

To solve such a problem the augmented ϵ-constraint method (AUGMECON) is adopted based on methodology introduced in [6]. AUGMECON is considered a posterior method in the sense that the decision-maker decides on the final solution after the Pareto optimal set is discovered. The advantage of this method over the weighted sum methods could be summarized in the following [29]:

1. AUGMECON can map the Pareto frontier for both convex and non-convex problems.
2. Unlike the weighted sum method the scaling of the objective function is not needed anymore.
3. Only unique non-dominated solutions are obtained in AUGMECON which results in a smaller number of iterations.
4. It uses lexicographic optimization to construct the pay-off table and determine the ranges of the objective functions to improve the efficiency of the optimal solution sets.
5. By eliminating the points with the same optimal solutions and/or infeasible solutions, the solving process is accelerated.

A generic multi-objective problem can be expressed as:

$$\max f_i(x) \qquad \forall i \in \mathcal{I} = \{1, 2, \dots, i_n\} \tag{2a}$$

$$s.t. \quad x \in \mathcal{X} \tag{2b}$$

The augmented single objective version of such a problem to be solved by AUGMECON is given in (3a)

$$\max f_1(x) + \sum_{i>1} \epsilon \left(10^{-(ord(i)-1)} \frac{s_i}{r_i} \right) \tag{3a}$$

$$s.t. \quad f_i(x) - s_i = e_i \qquad \forall i > 1 \tag{3b}$$

$$x \in \mathcal{X} \tag{3c}$$

where $f_1(x)$ is one of the multiple objectives (usually the first objective), s_i is the slack variable assigned for the objective functions with ϵ as the small constant value. Parameter e_i is the right-hand side (RHS) value that will be attained from the pay-off table which also reveals r_i the range of each objective function. The feasibility domain of the problem is defined by $\mathcal{X}$.

The solution methodology of such a multi-objective problem based on the AUGMECON is described briefly in Algorithm 1 based on [6].

Algorithm 1 AUGMECON algorithm for the multi-objective optimization problem.

1: Acquire objective function lists: $f(i)\ \forall i \in \mathcal{I}$
2: Create the lexicographic optimization-based payoff table (P) with $alias(i, j)$:
- for $i \in \mathcal{I}$: $P(i,i) = argmax\ f(i)\ ; f(i) == P(i,i)$
- for $i, j \in \mathcal{I} \mid i \neq j$: $P(i,j) = argmax\ f(i)\ ; f(j) == P(i,j)$

3: Obtain objective range $r(i)$ and the RHS value $e(i,k)$ for $k \in \mathcal{K}$ grid points:

$$r(i) = max(P(*,i)) - min(P(*,i))\ \forall i$$
$$e(i,k) = min(P(*,i)) + ord(k) \times r(i)/card(\mathcal{K})\ \forall k$$

4: Transform the problem to a single objective form shown in (3a).
5: Attain all the possible combinations of RHS value $e(i)$ based on the fixed number of grid points k for objective functions $f(i)\ \forall i > 1$:
- $E(c,i) = combine(e(i,*))\ \forall i > 1$
- The total number of combinations will be $card(c) = card(k)^{card(i)-1}$

6: Set RHS value in the problem (3a) to $e(i) = E(c,i)\ \forall c, i > 1$ and solve the sub-problem c to achieve the Pareto frontier.

As the summary of this section, the model presented in [28] focuses on optimizing short-term scheduling, with costs covering only operational expenses, excluding battery degradation in the optimization process. The Pareto optimal solutions generated by the Augmecon method prioritize minimizing daily operation costs and CO_2 emissions.

2.4. SOH as key performance indicator

From previous sections, both the battery physical model (Section 2.1), and the power curve of the battery, for each of the Pareto

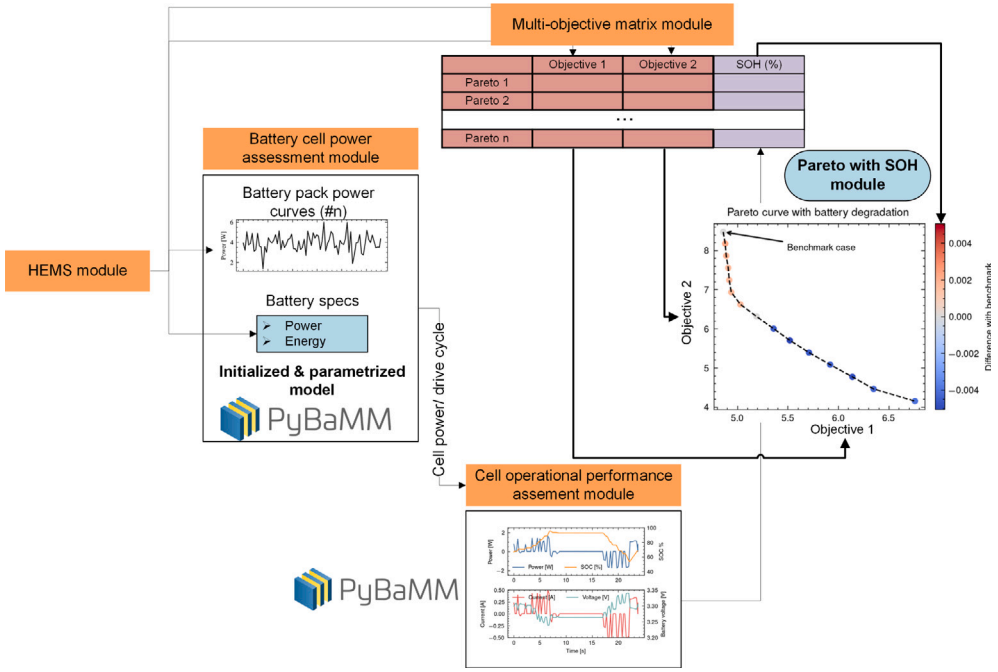

Fig. 7. Workflow of presented methodology, analyzing the Pareto curve using SOH as the performance indicator.

curve solutions (Section 2.3), are obtained. The complete workflow is depicted in Fig. 7. Where the battery cell power assessment module serves the purpose of converting power at the module level, sourced from HEMS, into the cell level. This distinction is vital as Pybamm operates at the cell level. On top of that, the electrical design of the battery cell-to-module must be carried out, with the already known cell characteristics (voltage, current, and capacity), provided by the manufacturer data-sheet and already parameterized previously. The design process is initiated by selecting the nominal voltage of the battery module, which, based on market standards, can typically be 12, 24, or 48 V. Following this, the capacity of the module is determined. However, for the sake of simplicity and given that designing the battery management system is not within the scope of this work, it is assumed that the battery power is equally distributed across each cell, as illustrated in Eqs. (4)–(6).

$$N_{cells,series} = \frac{V_{batt}}{V_{cell}} \tag{4}$$

$$N_{cells,parallel} = \frac{E_{batt}}{V_{batt} \cdot Q_{cell}} \tag{5}$$

$$p_{cell}(t) = \frac{p_{batt}(t)}{N_{cells,series} \cdot N_{cells,parallel}} \tag{6}$$

In Eq. (4), the number of cells in the battery module connected in series, of each parallel line, is evaluated using the battery voltage. Conversely, Eq. (5) is employed to determine the number of cell rows connected in parallel, based on the module energy (E_{batt}). Finally, assuming equal power distribution, Eq. (6) calculates the cell-level power curve derived from the battery module.

For each Pareto curve solution, there is a distinct power curve, meaning a distinct experiment for the parameterized model, with its own SOH indicator of the battery at the end of the evaluation time.

3. Results and analysis

In this section, the analyzed case, where LFP-type battery cells are adopted, based on the datasheet available, with 15 Pareto curve solutions based on two objectives, which are economical and environmental, for a multi-carrier energy system modeling, are reported.

Table 1
LFP Li-ion battery specifications.

Parameter	Value	Units
V_{nom}	3.2	V
$V_{up,cut}$	3.65	V
$V_{low,cut}$	2.5	V
I_{nom}	1.6	A
Q_{cell}	3.2	Ah
T_{op}	−20 ÷ 60	°C
$Crate_{max}$	3	–

Initially, this section illustrates the characteristics of the Li-ion cell and the parameterization process, focusing on the identification of the most influential model parameters. Subsequently, the section presents the results derived from 15 Pareto curve solutions, followed by an illustrative demonstration of the automatic selection of the optimal solution.

3.1. Cell characteristics

The cell characteristics are from the data-sheet of *CEGASA PORTABLE ENERGY*, available at [30], where its main specifications are reported in Table 1.

3.2. Parameterization

The initialization process is done through values from Table 1, with the Parameter set of *Prada2013* [23], Using SPMe modeling, as the best compromise between the accuracy and computational effort (Fig. 1), indeed it is an intermediate model between the simple single particle one and the complex two-dimensional model. The selection of the parameters is established according to the cell's chemistry, specifically Lithium Iron Phosphate (LFP). While Pybamm's developers offer this dataset, it is important to note that it is a composite of various sources. It is worth mentioning that even the developers themselves have acknowledged certain discrepancies within this dataset [27].

As outlined in the methodology section, the dataset's entire parameterization process can be logically divided into three distinct sections. In alignment with this structure, the results and corresponding comments are also organized accordingly.

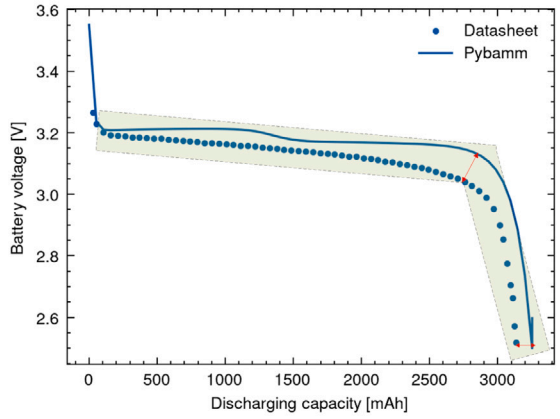

(a) Voltage drop difference between the standard Pybamm database data and the ones from [30]. Assessed using discharge curve with 1C at 298 K.

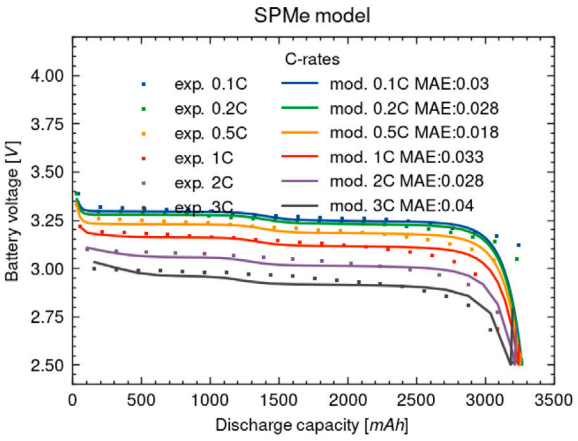

(b) Comparison between parameterized model, and the experimental data from datasheet [30], using the methodology presented in this work. Assessed with discharge curves with different C-rates at 298K.

Fig. 8. Electrochemical parameterization, using the data from [30].

3.2.1. Electrochemical parameterization

During the electrochemical parameterization process, two main inconsistencies from the initialized model and test results at different C-rates. (i) firstly the dischargeable energy from the cell is different from the nominal value, due to dataset inconsistencies, and (ii) the voltage drop slopes (Fig. 8(a)).

Addressing the first inconsistency is relatively straightforward. It involves adjusting the electrode geometry to match the required dischargeable capacity. Since dischargeable capacity is directly proportional to current density (A/m^2), and the current is determined by an internal formulation that is not easily accessible, altering the electrode's surface area offers a practical solution to achieve the desired outcome more efficiently. In contrast, resolving the voltage drop slope inconsistency is a more intricate process. It necessitates adopting the comprehensive approach described in Section 2.2.2. The key parameters to fine-tune in this case are the porosities of both the electrode and separator, which can vary between 0 and 1. These porosities are critical for ion transport within the battery and have been the subject of study for researchers like Parikh et al. [31]. Importantly, all three porosities are interconnected, making it challenging to isolate the effect of each one. Therefore, a grid search method is indispensable for this optimization process.

The results after the electrochemical parameterization are illustrated in Fig. 8(b), where the MAE is minimized for different C-rates.

3.2.2. Thermal parameterization

Regarding thermal parameterization, while for the Pouch form cells, many thermal models can be adopted, in the case of a cylindrical cell like the one adopted in this study, the "lumped thermal model" is the only choice offered [32]. This model treats the entire cylindrical cell as a single entity and characterizes it based on the thermal properties of the cell as a whole. Consequently, it does not capture the internal thermal behavior of the cell. However, this simplified approach aligns with the overarching objective of this work, which focuses on a systematic approach rather than an in-depth assessment of thermal behavior. Therefore, this assumption is acceptable for the purposes of this study.

Two different natures of the difference between the reported data in the data-sheet and the initialized model are observed:

1. The voltage gap, among different discharge curves at different working temperatures, enlarges when it is far from the reference temperature, and as

$$\Delta V = f(T) \tag{7}$$

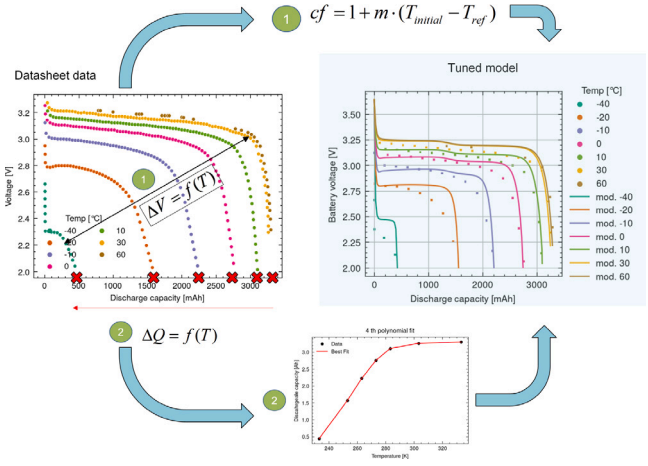

Fig. 9. Thermal parameterization represents the subsequent stage of electrochemical parameterization. Which is adjusted with the voltage gap (ΔQ) and decreasing capacity (cf) functions, based on the experimental data from datasheet.

A solution to this is to adopt a new temperature, adjusted with a correction factor that can manage such behavior, so that the model's input temperature is the new modified temperature. Of course, with such a process, the updated temperature does not have a physical meaning, and for temperature variation analysis the initial temperature is referenced.

$$T_{new} = T_{initial} \cdot cf \tag{8}$$

$$cf = 1 + m \cdot (T_{initial} - T_{ref}) \tag{9}$$

Such inconsistency is fixed using a correction factor (cf), which is a linear interpolation, which depends on the ΔT between the working temperature and the reference temperature (T_{ref} = 298.15 K)

2. Decreasing trend about the cell available capacity (Q), working at low temperatures:

$$\Delta Q = f(T) \tag{10}$$

In order to take this into account, the available capacity of the cell at different temperatures is gathered to be described through a polynomial function ($f(T)$), and as best polynomial

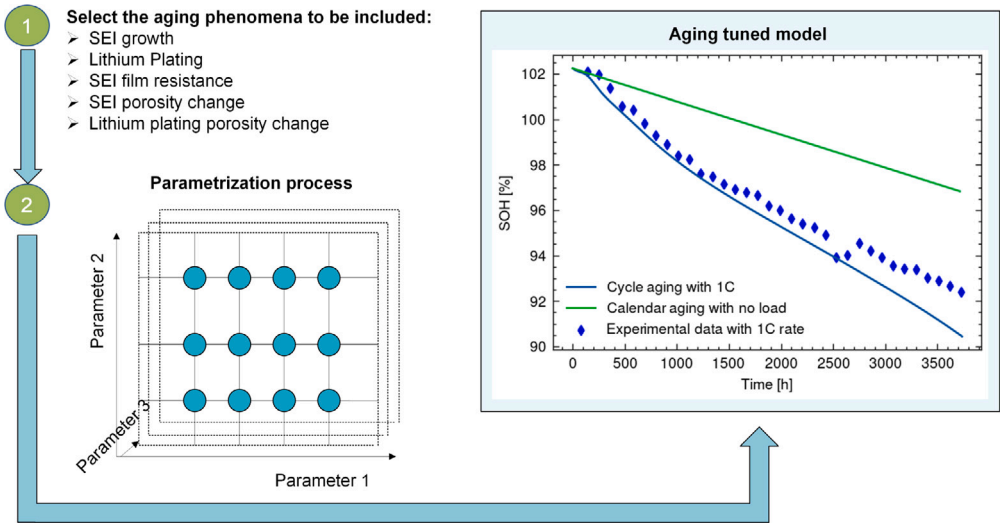

Fig. 10. The aging parameterization process is divided into two steps. Firstly, the aging phenomena, which capture the trend of the experimental data, are chosen. This is followed by parameter tuning using the experimental data from the datasheet.

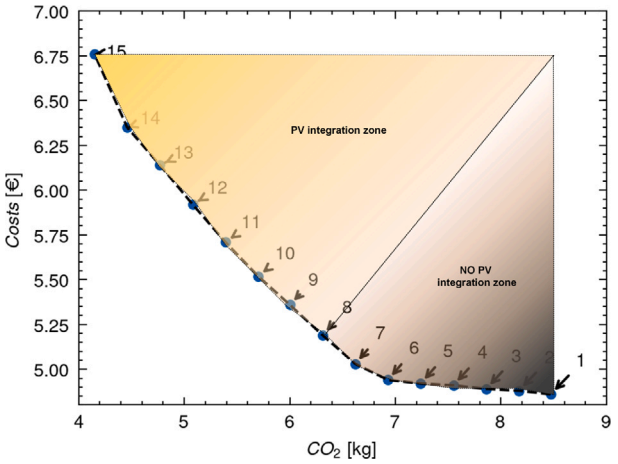

Fig. 11. The Pareto curve is derived from HEMS. In cases 1 to 8, there is no integration of PV systems, whereas in the remaining cases, PV systems are integrated, albeit at a higher economic cost.

order, i.e. compromise between the accuracy and complexity of it, results to be a 4th order, to describe such variation.

The entire thermal parameterization process is illustrated in Fig. 9, where the comparison is also reported, between the tuned model and the experimental data. As can be seen, although the different correction measures, the model cannot accurately describe the discharge curves at low temperatures (≤ 0 °C), where the second part of voltage drop (dV/dQ) happens much earlier than the model predicts. Despite of such differences, since the objective of the work is not thermal assessment, the cell is set to work at the reference temperature (298K).

3.2.3. Aging parameterization

Aging parameterization is arguably the most intricate aspect of this study, primarily owing to the inherent complexity of the phenomena involved. The aging behavior of Li-ion batteries constitutes a vast and exceedingly challenging research area, requiring diverse areas of expertise for a comprehensive understanding. Various authors have delved into the fundamental characteristics of aging in Li-ion batteries [33,34]. Additionally, it is noteworthy that the developers of Pybamm have conducted a detailed analysis of aging phenomena, which encompass the factors contributing to the gradual reduction in a cell's available capacity over time. These insights have been thoughtfully incorporated into the Pybamm framework [35], which are the following ones:

1. Solid-Electrolyte Interface (SEI) layer growth
2. Lithium plating
3. Particle fracture/cracking
4. Loss of active material

It is not frivolous to understand the coupling effects among different degradation phenomena, and it is out of the scope to investigate them, thus, in this work, the aim is to have the easiest approach, from a computational effort point of view, that guarantees a reasonable accuracy with experimental data. Furthermore, since the aging data requires extended experimental cycles (>2000), using a standard cycle, which is composed of a complete charge and discharge at 1C rate, its parameterization is extremely time-consuming, compared with the previous ones, which requires only half of the cycle (full discharge).

In the context of aging parameterization, it is crucial to begin by understanding which phenomena should be incorporated into the model. This necessitates a comparative analysis of various degradation behaviors to identify the one that aligns most closely with the experimental data. In the case study under consideration, the following aging phenomena have been taken into account: SEI growth, lithium plating, and alterations in lithium plating porosity. Once these aging phenomena have been defined, the entire parameterization process is executed in accordance with the method detailed in Section 2.2.2.

The full aging parameterization process is reported in Fig. 10, where the tuned model and its comparison with experimental data are also illustrated. Furthermore, calendar aging is predominant in such cells. Despite it is not common, calendar aging can prevail over cycle aging, which was also analyzed by other researchers previously [36,37], especially when cycle depths and current rates are low.

3.3. HEMS results

From the HEMS, a total of 15 optimal solutions are derived from the Pareto front, each employing distinct scheduling strategies. It is important to note that, given the primary focus of this work on the battery, only the power curve and state of charge of the battery are considered and extensively discussed in a dedicated section located in the appendix. Operating conditions of other technologies integrated into the HEMS are not documented in this study as they fall outside the scope of our investigation, as previously delineated in Fig. 7.

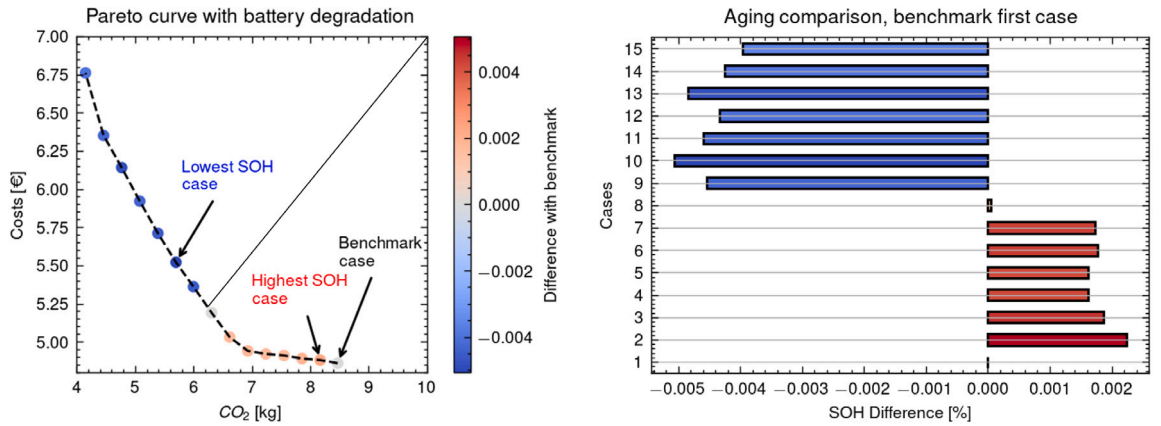

(a) Pareto curve of environmental and economic objectives. The colormap indicates the state of the health of the battery at the end of the day, compared with a benchmark case.

(b) State of Health difference among 15 solutions of Pareto curve, with 1st case as benchmark.

Fig. 12. SOH as Pareto indicator: While red solutions have more SOH the blue ones have less SOH, compared with the benchmark case. The differences among the different cases are extremely low due to the limited time frame of the study.

The Pareto curves generated by HEMS are visually represented in Fig. 11. This graphical representation allows the identification of, based on the battery power curves, which solutions effectively utilize Photovoltaic (PV) production. Notably, solutions (1–7) do not absorb the PV production, resulting in increased carbon emissions during the day. Conversely, in other cases, the effort to reduce emissions necessitates higher economic expenses.

3.4. Pareto curve assessment

With the parameterized Pybamm model, and the battery power curve from HEMS, is possible therefore to perform the experiments based on different drive cycles. For the sake of simplicity, the cell-level power curve is simply the pack-level power curve scaled with the number of cells, and the whole battery configuration is reported in Table 3. Thus, 15 different experiments are performed using Pybamm, obtaining different SOH at the end of the evaluation time frame. Notably, due to the choice of a constrained evaluation window lasting 24 h, this duration was insufficient to induce substantial battery degradation. To facilitate a comparative analysis of these solutions, it is established a benchmark case.

The process of automatically selecting the ultimate case using a portable computer took approximately 10 min. Detailed specifications regarding computational resources and the case study are provided in the appendix section, Table 4. While the results are visually depicted in Figs. 12. Fig. 12(a) presents a color map illustrating the SOH difference among the 15 Pareto frontier solutions, using it as a KPI. In general, solutions without PV integration tend to have higher SOH compared to the benchmark case. Notably, Case 8 represents a solution that effectively divides the Pareto frontier into two distinct zones. However, it is not a straightforward relationship where more PV penetration necessarily means lower SOH. In fact, Case 2 has the maximum SOH despite not having the least PV integration. Therefore, from a real-time scheduling perspective, the operational strategy employed in Case 2 emerges as the ultimate solution among all optimal scenarios. This strategy ensures the maximum health of the battery at the end of the evaluation time.

4. Conclusions

In this study, a novel approach is introduced, to automatically identify the best solution from a set of optimal solutions within the Pareto frontier, as a result of multi-objective problems in multi-energy systems. The proposed approach specifically focuses on battery technology, leveraging the State of Health as a key indicator. The SOH is evaluated using a parameterized physical model through the use of experimental data from the manufacturer's datasheet. While similar works by other researchers have adopted comparable approaches, using different indicators like grid independence or customer satisfaction, the focus here is on battery degradation evaluation. This evaluation is particularly challenging, as highlighted in the literature, making the proposed methodology a valuable contribution to the field.

Moreover, to assess the potential and limitations of the proposed methodology, a case study is conducted. In this case study, a two-objective scheduling problem is solved within a multi-carrier Home Energy Management System framework, Specifically economic and environmental objectives are considered. The study incorporates 15 optimal solutions obtained from the optimization process, which are then used to conduct experiments with the parameterized physical battery model. Through these experiments, the efficacy and applicability of the proposed methodology are examined and evaluated.

The parameterization of the battery cell is divided into three different stages, to capture different physical behaviors of the cell, which are (i) electrochemical (ii) thermal, and (iii) aging respectively, all three stages are interconnected, yet they can be done sequentially. The data-driven approach has been adopted for the parameterization process, comparing the model's results and experimental data declared by the cell manufacturer, in order to tune the model accordingly; While the electrochemical parameterization is sufficient to tune the several parameters, for the other two stages instead, additional functions have to be included, based on the difference among the model and experimental data, which requires comprehensive knowledge about the physical model's equations and structure, supported by a proper data analysis about the experimental data of the manufacturers in order to properly correct the behavior. Thus, the parameterization is the most arduous and time-consuming part of the whole methodology.

The results affirm the suitability of the proposed methodology for automatically determining the optimal solution, employing SOH as a performance metric. Overextended operational periods, such as 10 years, with consistent scheduling strategies, this approach can yield savings of up to 26.67% in battery lifespan. This is particularly significant in the context of multi-energy systems economics, given the frequency of battery replacements and its related investment costs. It is worth noting that while integrating PV systems can accelerate battery degradation due to increased usage, it is not immediately evident that the highest PV integration (case 15) leads to the worst SOH. In fact, the 10th scenario in the case study represents the worst SOH case,

Table 2
HEMS results: battery.

Parameter	Value	Units
Energy	15	kWh
Nominal power	3	kW
Minimum SOC	20	%
Maximum C-rate	0.25	C

Table 3
Battery module design specs.

Rack configuration	#10 modules in parallel
Module specs	
Configuration	4S40P
Voltage	12 V
Capacity	128 Ah

as illustrated in Fig. 12(a). Therefore, the utilization of SOH as a key indicator provides valuable insights. Furthermore, it is important to highlight that the analysis reported only considers stationary battery energy storage. However, the same methodology can be extended to encompass electric vehicles, which can effectively function as a type of mobile battery storage. This extension could have even more significant implications for the overall system.

The process of parametrizing the Li-ion cell is undeniably time-consuming, and its duration cannot be precisely estimated due to its inherent complexity. However, the Python-based architecture of Pybamm offers a practical advantage: once the parameters are determined and stored, they can be readily applied to any number of experiments involving the same type of cells. This eliminates the need to repeat the entire parameterization process for each subsequent study.

In the case study, a one-day evaluation time window was chosen to validate the methodology, primarily for computational efficiency. Nonetheless, it is important to note that this relatively short timeframe has a limited impact on battery degradation. In future research endeavors, simulations over a more extended period are planned. While this approach will entail greater computational demands, it will provide a more comprehensive understanding of battery behavior over time. Moreover, although the proposed approach has the novelty of automatic selection of the best solution from the Pareto curve, it also establishes a connection between battery operational parameters, such as SOH, and the optimization and scheduling problem of energy modeling. Nevertheless, it is important to acknowledge that the approach remains passive, in the sense that the SOH assessment and scheduling are conducted independently. Thus, there is a possibility to look for active integration, whereby the SOH derived from the Pybamm model serves as an indicator directly considered during the energy modeling optimization problem. With active integration, it would provide information that can directly influence the outputs of the optimization process.

CRediT authorship contribution statement

Lingkang Jin: Writing – original draft, Methodology, Investigation, Formal analysis, Data curation. **Milad Kazemi:** Writing – original draft, Resources, Formal analysis, Data curation. **Gabriele Comodi:** Writing – review & editing, Supervision. **Christina Papadimitriou:** Writing – review & editing, Supervision, Methodology, Conceptualization.

Declaration of competing interest

The authors declare that they have no known competing financial interests or personal relationships that could have appeared to influence the work reported in this paper.

Data availability

Data will be made available on request.

Appendix

In this section, all support materials for this work are presented. These materials include details on battery design characteristics, the rack design of battery modules, computational efforts, case study specifics, tuned parameters, as well as some experimental results from Pybamm (including voltage, current, and SOH) (see Figs. 13–15 and Tables 2 and 5).

Table 4
Computational specs for the case study.

Computation specs	
Model	Dell G5 15
CPU	Intel(R) Core(TM) i7-8750H CPU @ 2.20 GHz
RAM	8 Gb
Computation time	9 min 56 seconds
Case study details	
#n of scenarios	15
Time resolution	15 mins
Time horizon	24 h

Table 5
Pybamm model tuned parameters.

Parameter	Value	Units
Initialization dataset		
Prada2013	–	–
Electrochemical parameterization		
Positive electrode porosity	0.85	–
Separator porosity	0.04	–
Negative electrode porosity	0.3	–
Thermal parameterization		
$Q = aT^4 + bT^3 + cT^2 + dT + e$		
a	2.005e−07	–
b	−2.25933 e-04	–
c	9.443e−02	–
d	−1.732 e+01	–
e	1.177 e+03	–
$T_{new} = cf \cdot T_{initial}$		
$cf = 1 + m \cdot (T_{initial} - T_{ref})$		
m	0.006	–
T_{ref}	298.15	K
Aging parameterization		
SEI : ec reaction limited		
SEI growth activation energy	0	J/mol
EC initial concentration in electrolyte	4541	mol/m^3
SEI open-circuit potential	0.4	V
SEI resistivity	200 000	ohm/m
Initial outer SEI thickness	0.5e−9	m
Initial inner SEI thickness	2.5e−9	m
EC diffusivity	2e−18	m^2/s
Inner SEI reaction proportion	0.5	–
SEI reaction exchange current density	1.5e−07	A/m^2
Inner SEI partial molar volume	9.585e−05	m^3/mol
Ratio of lithium moles to SEI moles	2.0	–
Outer SEI partial molar volume	9.585e−05	m^3/mol
SEI kinetic rate constant	8.45e−17	m/s
Positive electrode active material volume fraction	0.295	–
Lithium plating : irreversible		
Exchange-current density for plating	0.00205	A/m^2
Typical plated lithium concentration	1000.0	mol/m
Initial plated lithium concentration	0	mol/m
Lithium plating transfer coefficient	3.0	–
Lithium plating porosity change : true		
Lithium metal partial molar volume	1.3e−05	m^3/mol

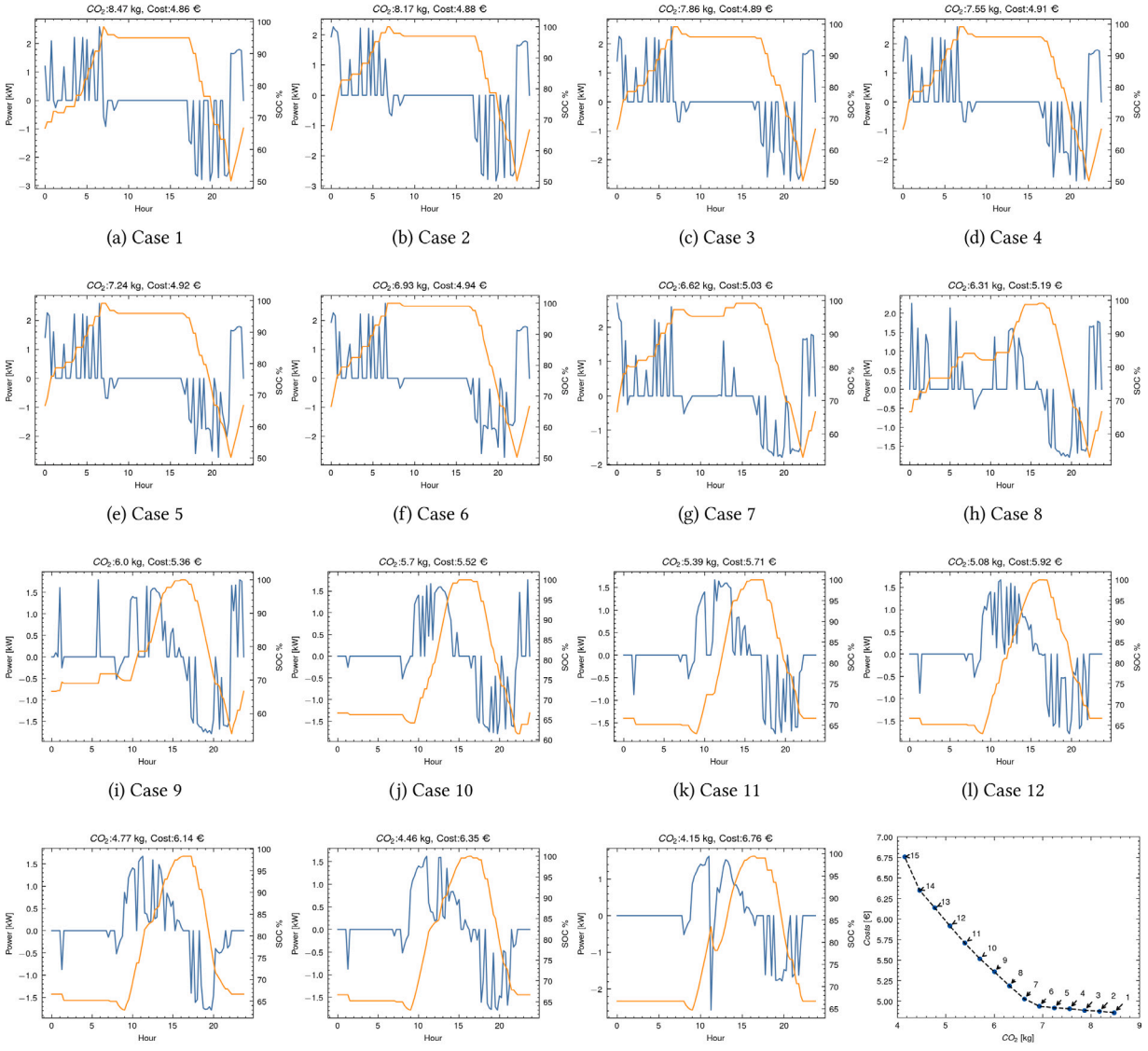

(a) Case 1 (b) Case 2 (c) Case 3 (d) Case 4

(e) Case 5 (f) Case 6 (g) Case 7 (h) Case 8

(i) Case 9 (j) Case 10 (k) Case 11 (l) Case 12

(m) Case 13 (n) Case 14 (o) Case 15 (p) Pareto curve

Fig. 13. HEMS results and Pareto curve.

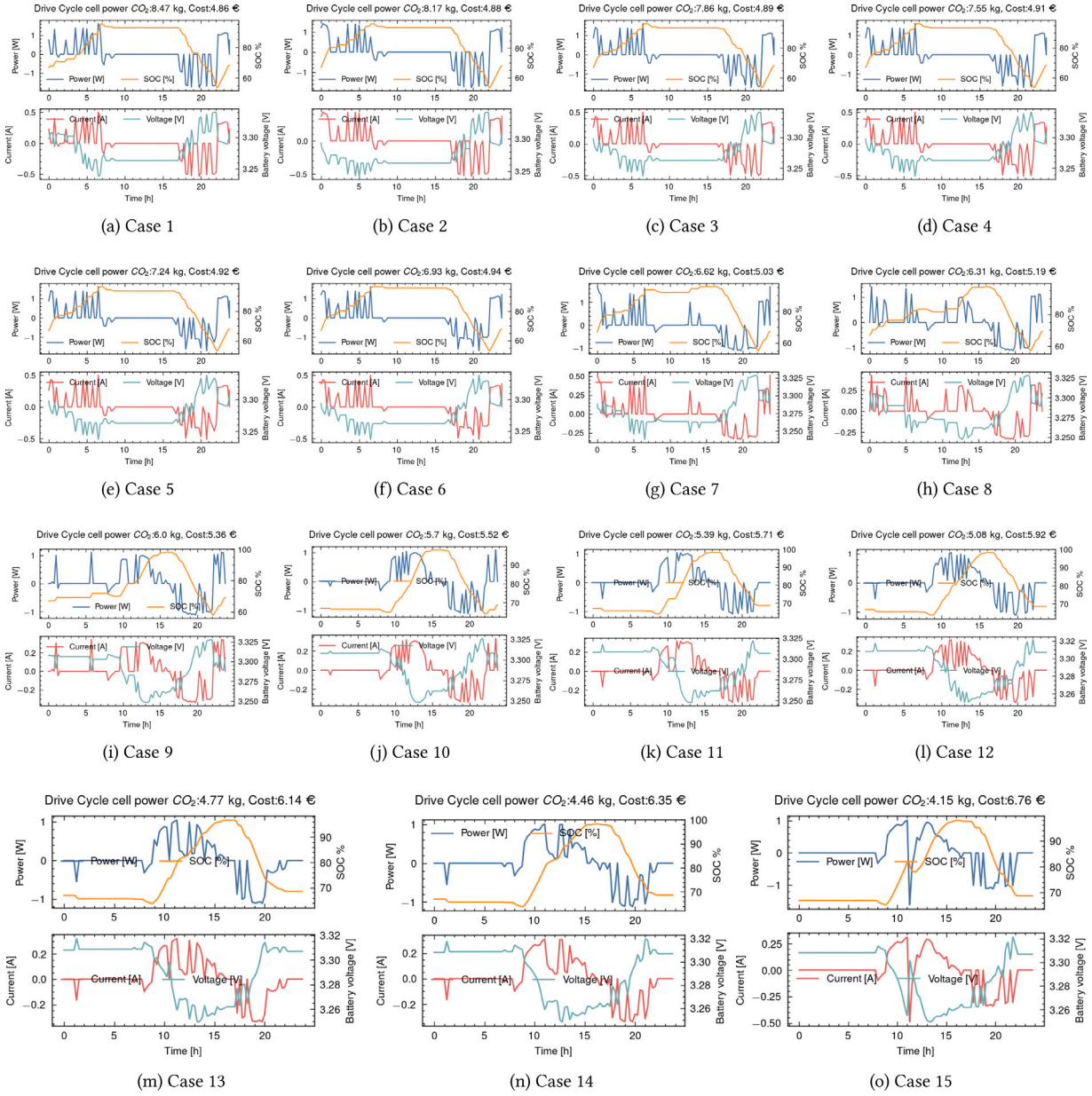

(a) Case 1 (b) Case 2 (c) Case 3 (d) Case 4

(e) Case 5 (f) Case 6 (g) Case 7 (h) Case 8

(i) Case 9 (j) Case 10 (k) Case 11 (l) Case 12

(m) Case 13 (n) Case 14 (o) Case 15

Fig. 14. Pybamm experiments: voltage and current.

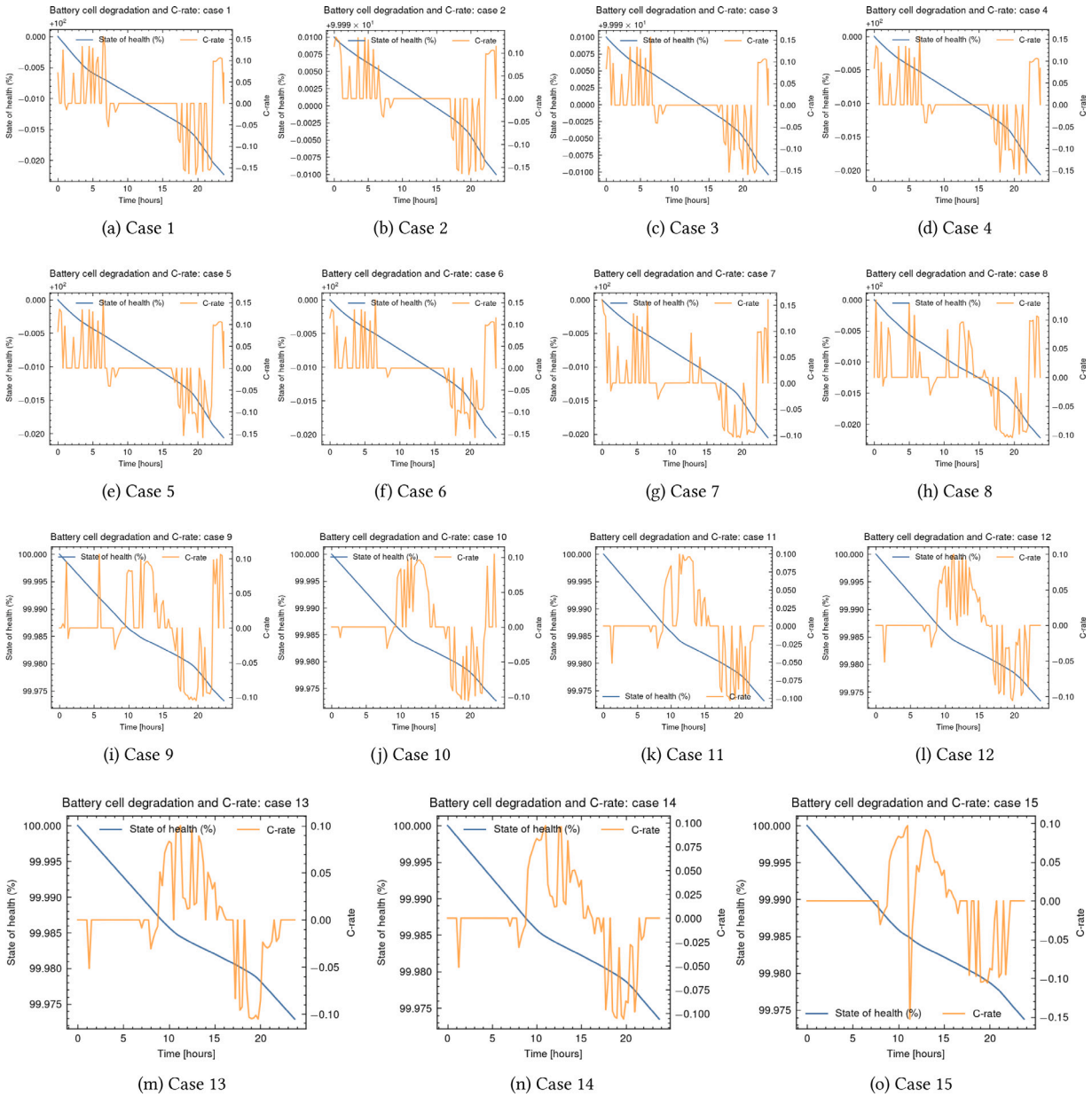

(a) Case 1 (b) Case 2 (c) Case 3 (d) Case 4

(e) Case 5 (f) Case 6 (g) Case 7 (h) Case 8

(i) Case 9 (j) Case 10 (k) Case 11 (l) Case 12

(m) Case 13 (n) Case 14 (o) Case 15

Fig. 15. Pybamm experiments: SOH and C-rate.

References

[1] Chang M, Thellufsen JZ, Zakeri B, Pickering B, Pfenninger S, Lund H, et al. Trends in tools and approaches for modelling the energy transition. Appl Energy 2021;290:116731. http://dx.doi.org/10.1016/J.APENERGY.2021.116731.

[2] Nuffel LV, Dedecca JG, Smit T, Rademaekers K. Sector coupling: how can it be enhanced in the EU to foster grid stability and decarbonise?. 2018, p. 1–151, November.

[3] Comodi G, Rossi M, Jin L, Ferrario AM, Ferracuti F, Alessia A, et al. Deliverable 2.2 Technical solutions for multi carrier integrated systems under the LEC concept: A review. 2021, URL https://eneuron.eu/wp-content/uploads/2022/02/D2.2_Technical-solutions-for-multi-carrier-integrated-systems-under-the-LEC-concept_A-review.pdf.

[4] Fiorini L, Aiello M. Automatic optimal multi-energy management of smart homes. Energy Inform 2022;5(1):1–20. http://dx.doi.org/10.1186/S42162-022-00253-0/TABLES/10, URL https://energyinformatics.springeropen.com/articles/10.1186/s42162-022-00253-0.

[5] Khezri R, Mahmoudi A. Review on the state-of-the-art multi-objective optimisation of hybrid standalone/grid-connected energy systems. IET Gener Transm Distrib 2020;14(20):4285–300. http://dx.doi.org/10.1049/IET-GTD.2020.0453, URL https://onlinelibrary.wiley.com/doi/full/10.1049/iet-gtd.2020.0453.

[6] Mavrotas G. Effective implementation of the ϵ-constraint method in Multi-Objective Mathematical Programming problems. Appl Math Comput 2009;213(2):455–65. http://dx.doi.org/10.1016/j.amc.2009.03.037, URL http://dx.doi.org/10.1016/j.amc.2009.03.037.

[7] Papadimitriou C, Charalampous C, Bracho J, Borray AFC. 2022. D4.1_Report-on-the-energy-hub-concept-and-the-multi-objective-programming-approach-of-an-energy-hubURL https://eneuron.eu/wp-content/uploads/2022/06/D4.1_Report-on-the-energy-hub-concept-and-the-multi-objective-programming-approach-of-an-energy-hub.pdf.

[8] Wang Z, Rangaiah GP. Application and analysis of methods for selecting an optimal solution from the Pareto-optimal front obtained by multiobjective optimization. Ind Eng Chem Res 2017;56(2):560–74. http://dx.doi.org/10.1021/ACS.IECR.6B03453/ASSET/IMAGES/LARGE/IE-2016-03453R{_}0010.JPEG, URL https://pubs.acs.org/doi/full/10.1021/acs.iecr.6b03453.

[9] Tian H, Qin P, Li K, Zhao Z. A review of the state of health for lithium-ion batteries: Research status and suggestions. J Clean Prod 2020;261. http://dx.doi.org/10.1016/j.jclepro.2020.120813.

[10] Ng MF, Zhao J, Yan Q, Conduit GJ, Seh ZW. Predicting the state of charge and health of batteries using data-driven machine learning. Nat Mach Intell 2020;2(3):161–70. http://dx.doi.org/10.1038/s42256-020-0156-7.

[11] Doyle M, Fuller TF, Newman J. Modeling of galvanostatic charge and discharge of the lithium/polymer/insertion cell. J Electrochem Soc 1993;140(6):1526–33. http://dx.doi.org/10.1149/1.2221597/XML, https://iopscience.iop.org/article/10.1149/1.2221597. https://iopscience.iop.org/article/10.1149/1.2221597/meta.

[12] Fuller TF, Doyle M, Newman J. Simulation and optimization of the dual lithium ion insertion cell. J Electrochem Soc 1994;141(1):1–10. http://dx.doi.org/10.1149/1.2054684.
[13] Yang S, Zhang C, Jiang J, Zhang W, Zhang L, Wang Y. Review on state-of-health of lithium-ion batteries: Characterizations, estimations and applications. J Clean Prod 2021;314. http://dx.doi.org/10.1016/j.jclepro.2021.128015.
[14] Sulzer V, Marquis SG, Timms R, Robinson M, Chapman SJ. Python battery mathematical modelling (PyBaMM). J Open Res Softw 2021;9(1):1–8. http://dx.doi.org/10.5334/JORS.309, URL https://openresearchsoftware.metajnl.com/articles/10.5334/jors.309.
[15] Multi-Scale Modelling - The Faraday Institution. URL https://www.faraday.ac.uk/research/lithium-ion/battery-system-modelling/.
[16] NumFOCUS: A Nonprofit Supporting Open Code for Better Science. URL https://numfocus.org/.
[17] pybamm-team/PyBaMM: Fast and flexible physics-based battery models in Python. URL https://github.com/pybamm-team/PyBaMM.
[18] Marquis SG, Sulzer V, Timms R, Please CP, Chapman SJ. An asymptotic derivation of a single particle model with electrolyte. J Electrochem Soc 2019;166(15):A3693–706. http://dx.doi.org/10.1149/2.0341915JES/XML, https://iopscience.iop.org/article/10.1149/2.0341915jes. https://iopscience.iop.org/article/10.1149/2.0341915jes/meta.
[19] Andersson JA, Gillis J, Horn G, Rawlings JB, Diehl M. CasADi: a software framework for nonlinear optimization and optimal control. Math Program Comput 2019;11(1):1–36. http://dx.doi.org/10.1007/S12532-018-0139-4/TABLES/3, URL https://link.springer.com/article/10.1007/s12532-018-0139-4.
[20] Li J, Zou L, Tian F, al -, Mishra A, Subramanian VR, et al. Development of experimental techniques for parameterization of multi-scale lithium-ion battery models. J Electrochem Soc 2020;167(8):80534. http://dx.doi.org/10.1149/1945-7111/AB9050, https://iopscience.iop.org/article/10.1149/1945-7111/ab9050. https://iopscience.iop.org/article/10.1149/1945-7111/ab9050/meta.
[21] Mohtat P, Lee S, Siegel JB, Stefanopoulou AG. Towards better estimability of electrode-specific state of health: Decoding the cell expansion. J Power Sources 2019;427:101–11. http://dx.doi.org/10.1016/J.JPOWSOUR.2019.03.104.
[22] Nyman A, Behm M, Lindbergh G. Electrochemical characterisation and modelling of the mass transport phenomena in LiPF6–EC–EMC electrolyte. Electrochim Acta 2008;53(22):6356–65. http://dx.doi.org/10.1016/J.ELECTACTA.2008.04.023.
[23] Prada E, Domenico DD, Creff Y, Bernard J, Sauvant-Moynot V, Huet F. A simplified electrochemical and thermal aging model of LiFePO 4 - graphite Li-ion batteries: Power and capacity fade simulations. J Electrochem Soc 2013;160(4):A616–28. http://dx.doi.org/10.1149/2.053304JES/XML, https://iopscience.iop.org/article/10.1149/2.053304jes. https://iopscience.iop.org/article/10.1149/2.053304jes/meta.
[24] Weng A, Siegel JB, Stefanopoulou A. Differential voltage analysis for battery manufacturing process control. 2023, http://dx.doi.org/10.3389/fenrg.2023.1087269, URL https://arxiv.org/abs/2303.07088v1.
[25] Berliner MD, Cogswell DA, Bazant MZ, Braatz RD. Methods-PETLION: Open-source software for millisecond-scale porous electrode theory-based lithium-ion battery simulations. 2021, http://dx.doi.org/10.1149/1945-7111/ac201c.
[26] GitHub - MarcBerliner/PETLION.jl: High-performance simulations of the Porous Electrode Theory for Li-ion batteries. URL https://github.com/MarcBerliner/PETLION.jl.
[27] Parameters Sets — PyBaMM v23.4.1 Manual. URL https://pybamm.readthedocs.io/en/latest/source/api/parameters/parameter_sets.html.
[28] Kazemi M, Papadimitriou C, Paterakis N, Kok K, Dukovska I. Optimal design of multi-carrier and -objective home energy management system. In: IEEE sEST. Mugla, Turkey; 2023, p. 1–6.
[29] Paterakis NG, Mazza A, Santos SF, Erdinc O, Chicco G, Bakirtzis AG, et al. Multi-objective reconfiguration of radial distribution systems using reliability indices. IEEE Trans Power Syst 2016;31(2):1048–62. http://dx.doi.org/10.1109/TPWRS.2015.2425801.
[30] CEGASA. LFP Cell datasheet. URL https://www.google.com/url?sa=t&rct=j&q=&esrc=s&source=web&cd=&cad=rja&uact=8&ved=2ahUKEwjNnbfF14mDAxX82wIHHaPTAiMQFnoECBIQAQ&url=https%3A%2F%2Fe2e.ti.com%2Fcfs-file%2F_key%2Fcommunityserver-discussions-components-files%2F196%2FP3_2D00_Datasheet-Cell-_2D00_3232-LFP-26650.pdf&usg=AOvVaw3bEBjO5GcokLzx1MuwVzjE&opi=89978449.
[31] Parikh D, Christensen T, Li J. Correlating the influence of porosity, tortuosity, and mass loading on the energy density of LiNi0.6Mn0.2Co0.2O2 cathodes under extreme fast charging (XFC) conditions. J Power Sources 2020;474(C). http://dx.doi.org/10.1016/J.JPOWSOUR.2020.228601.
[32] Thermal models — PyBaMM v23.9 Manual. URL https://docs.pybamm.org/en/stable/source/examples/notebooks/models/thermal-models.html.
[33] Vermeer W, Chandra Mouli GR, Bauer P. A comprehensive review on the characteristics and modeling of lithium-ion battery aging. IEEE Trans Transp Electrif 2022;8(2):2205–32. http://dx.doi.org/10.1109/TTE.2021.3138357.
[34] Edge JS, O'Kane S, Prosser R, Kirkaldy ND, Patel AN, Hales A, et al. Lithium ion battery degradation: what you need to know. Phys Chem Chem Phys 2021;23(14):8200–21. http://dx.doi.org/10.1039/D1CP00359C, https://pubs.rsc.org/en/content/articlehtml/2021/cp/d1cp00359c. https://pubs.rsc.org/en/content/articlelanding/2021/cp/d1cp00359c.
[35] O'Kane SE, Ai W, Madabattula G, Alonso-Alvarez D, Timms R, Sulzer V, et al. Lithium-ion battery degradation: how to model it. Phys Chem Chem Phys 2022;24(13):7909–22. http://dx.doi.org/10.1039/D2CP00417H, https://pubs.rsc.org/en/content/articlehtml/2022/cp/d2cp00417h. https://pubs.rsc.org/en/content/articlelanding/2022/cp/d2cp00417h.
[36] Keil P, Wilhelm J, Schuster S. Calendar aging of lithium-ion batteries you may also like insights on calendar aging of lithium-ion batteries from differential voltage analysis and coulometry. http://dx.doi.org/10.1149/2.0411609jes.
[37] Redondo-Iglesias E, Venet P, Pelissier S. Calendar and cycling ageing combination of batteries in electric vehicles. Microelectron Reliab 2018;88–90:1212–5. http://dx.doi.org/10.1016/J.MICROREL.2018.06.113.